Earth and Planetary Science Letters 444 (2016) 34–44

Contents lists available at ScienceDirect

Earth and Planetary Science Letters

www.elsevier.com/locate/epsl

The impact of glacier retreat from the Ross Sea on local climate: Characterization of mineral dust in the Taylor Dome ice core, East Antarctica

S.M. Aarons [a,*], S.M. Aciego [a], P. Gabrielli [b,c], B. Delmonte [d], J.M. Koornneef [e], A. Wegner [a,f], M.A. Blakowski [a]

[a] Glaciochemistry and Isotope Geochemistry Lab, University of Michigan, 1100 N. University Ave, Ann Arbor, MI, 48109, USA
[b] Byrd Polar and Climate Research Center, The Ohio State University, 108 Scott Hall, 1090 Carmack Road, Columbus, OH, 43210, USA
[c] School of Earth Sciences, The Ohio State University, 275 Mendenhall Laboratory, 125 South Oval Mall, Columbus, OH, 43210, USA
[d] Disat, University of Milano-Bicocca, Piazza della Scienza 1, Milan, 20126, Italy
[e] Vrije University Amsterdam, de Boelelaan 1085, 1081HV Amsterdam, The Netherlands
[f] Stiftung Alfred-Wegener-Institut für Polar- und Meeresforschung, Am Alten Hafen 26, Bremerhaven, 27568, Germany

ARTICLE INFO

Article history:
Received 30 June 2015
Received in revised form 6 March 2016
Accepted 20 March 2016
Available online xxxx
Editor: M. Frank

Keywords:
Antarctica
dust
ice core
strontium
neodymium
rare earth elements

ABSTRACT

Recent declines in ice shelf and sea ice extent experienced in polar regions highlight the importance of evaluating variations in local weather patterns in response to climate change. Airborne mineral particles (dust) transported through the atmosphere and deposited on ice sheets and glaciers in Antarctica and Greenland can provide a robust set of tools for resolving the evolution of climatic systems through time. Here we present the first high time resolution radiogenic isotope (strontium and neodymium) data for Holocene dust in a coastal East Antarctic ice core, accompanied by rare earth element composition, dust concentration, and particle size distribution during the last deglaciation. We aim to use these combined ice core data to determine dust provenance, with variations indicative of shifts in either dust production, sources, and/or transport pathways. We analyzed a series of 17 samples from the Taylor Dome (77°47′47″S, 158°43′26″E) ice core, 113–391 m in depth from 1.1–31.4 ka. Radiogenic isotopic and rare earth element compositions of dust during the last glacial period are in good agreement with previously measured East Antarctic ice core dust records. In contrast, the Holocene dust dataset displays a broad range in isotopic and rare earth element compositions, suggesting a shift from long-range transported dust to a more variable, local input that may be linked to the retreat of the Ross Ice Shelf during the last deglaciation. Observed changes in the dust cycle inferred from a coastal East Antarctic ice core can thus be used to infer an evolving local climate.

1. Introduction

Fluctuations in the amount and/or extent of sea ice and ice shelves alter wind speed and direction, as well as local storm trajectories (Vihma, 2014; Francis et al., 2009). Modeling the interaction between ice sheets and local climate demonstrates that air is cooled locally over an ice sheet, affecting the atmospheric flow response (Liakka and Nilsson, 2010). The high albedo and altitude of ice sheets can induce zonal anomalies in surface temperature, which can modify large-scale atmospheric circulation (Cook and Held, 1988; Beghin et al., 2014). Furthermore, several studies have implied that an ice sheet is capable of changing the position of the subtropical jet, in turn altering storm trajectories (Hall et al., 1996; Kageyama and Valdes, 2000; Laîné et al., 2008; Rivière et al., 2010). The change in storm trajectories will undoubtedly result in changes in precipitation pathways and the ice accumulation rates over ice sheets (Beghin et al., 2014). It is possible that variations in the extent of glaciation, sea-ice and ice shelves are capable of driving significant atmospheric climatic variations on seasonal, decadal, millennial and glacial–interglacial cycles.

Ice cores from the Antarctic ice sheet provide records of past climate extending over hundreds of thousands of years (Jouzel et al., 1995; Petit et al., 1999). Chemical and mineralogical characterization of dust particles transported through the atmosphere and deposited on ice sheets and glaciers allow for the reconstruction

* Corresponding author.
E-mail address: smaarons@umich.edu (S.M. Aarons).

http://dx.doi.org/10.1016/j.epsl.2016.03.035
0012-821X/

of regional and global climate patterns. The dust concentration and composition of long timescale ice cores varies with air temperature as recorded by stable isotopes: previous studies have established that dust concentration is one-to-two orders of magnitude greater during glacial versus interglacial periods. The increased dust deposition may be attributed to higher dust availability at source areas and higher wind speeds caused by a stronger equator to pole temperature gradient (Hammer et al., 1985; Delmonte et al., 2004a), or stronger wind gusts in dust source regions during periods of steepened meridonal temperature gradients (McGee et al., 2010). Provenance of dust deposited in ice can be characterized using radiogenic isotopes, including strontium ($^{87}Sr/^{86}Sr$), neodymium ($^{143}Nd/^{144}Nd$), hafnium ($^{176}Hf/^{177}Hf$) (Grousset and Biscaye, 2005; Basile et al., 1997; Delmonte et al., 2004a, 2004b, 2008; Lupker et al., 2010), and REE concentration (Wegner et al., 2012). The isotopic composition of ice core dust compared to Potential Source Areas (PSAs) of windborne material indicate variations in the dust provenance (Delmonte et al., 2004a; Wolff et al., 2006), which may be used to resolve past climate changes. The longest timescale ice core records are from interior East Antarctica (Petit et al., 1999), yet ice cores from coastal East Antarctic sites (i.e. Talos Dome) are capable of providing undisturbed, detailed records of the last climatic cycle in a region of the East Antarctic ice sheet with distinctive climate conditions (Delmonte et al., 2010).

Previous work on central and coastal east Antarctic ice cores identify southern South America (SSA) as the most likely source of windblown mineral dust during late Quaternary glacial periods. The size distribution and chemical composition of dust from interglacial periods is more variable and in coastal ice cores may potentially originate from local sources, although analytical limitations have made correlating interglacial ice core dust to source area challenging (Delmonte et al., 2007, 2010; Gabrielli et al., 2010).

In 1992, a ~554 m deep ice core was retrieved at Taylor Dome (TYD) (M3C1 ice core, 77°47′47″S; 158°43′26″E, 2365 m a.s.l.), a local ice-accumulation area for the Taylor Glacier. TYD is located on the eastern margin of the East Antarctic ice sheet (Fig. 1), in close proximity to the current position of the Ross Ice Shelf and seasonal sea ice of the Ross Sea. The TYD core was the third ice core (following Vostok and the first Dome C core) to provide a stratigraphically intact record of the Holocene through the last glacial cycle, going back to ~130 ka (Grootes et al., 1994; Steig et al., 2000).

Katabatic-driven movements of cold interior Antarctica air masses approaching from the southwest largely influences the weather at TYD (Morse et al., 1998), whereas warmer, precipitation-laden air masses approach TYD from the south (Morse, 1997). The latter air masses are linked to cyclones originating near Marie Byrd Land (Fig. 1), traveling over the Ross Ice Shelf and across the Transantarctic Mountains before deposition at TYD (Harris, 1992).

During the Last Glacial Maximum (LGM), the accumulation rate at TYD drastically decreased, suggesting a change in atmospheric circulation during the late ice age period (Morse et al., 1998). Morse et al. (1998) hypothesized that moisture-bearing storms arrived at TYD from the north (rather than the south as they do presently), a result of changing ice cover in the Ross Embayment. The elevated topography in the Ross Embayment (e.g. from the Ice Shelf or Ross 'Ice Sheet') and northward displacement of the Ross Low combined to displace the storm tracks northward through the Transantarctic Mountains north of the Royal Society Range (Morse et al., 1998) (Fig. 1). Terrestrial and marine geological evidence indicates that grounded ice advanced far into the Ross Sea during the Last Glacial Period (LGP), reaching its greatest thickness and extent between 12.8–18.7 ka (Hall et al., 2015). The recession of the ice sheet began about 12.8 ka, and it retreated from the McMurdo

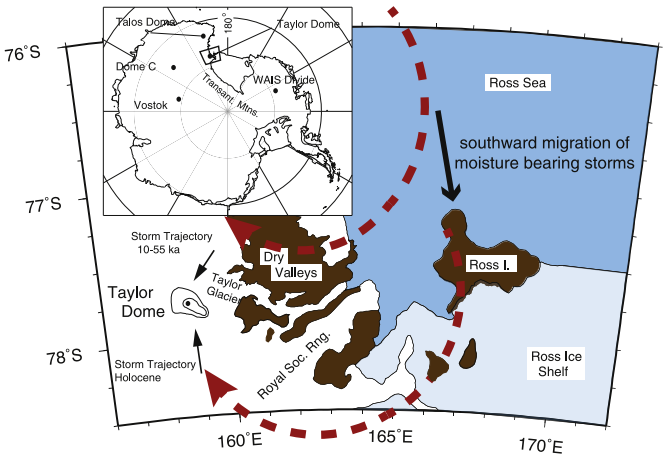

Fig. 1. Map of Taylor Dome and surrounding area, with major ice core drilling sites and the hypothesized Last Glacial Maximum (top dashed arrow) and current Holocene (bottom dashed arrow) storm trajectory (figure adapted from Morse et al., 1998).

Sound area over the period 11.5–6 ka (Anderson et al., 1992; Licht et al., 1996), aligned with the proposed timeline for southerly storm trajectories.

We utilize the TYD ice core dust record to examine the changes in local weather and storm trajectories during and following the retreat of the Ross Ice Shelf during the last deglaciation. Dry and windy conditions throughout the LGP are likely to have established the dominance of dry-deposited dust on TYD, as opposed to sea-salt aerosol. The dust accumulation rates should have decreased throughout the last deglaciation, and the sources and transport pathways of dust may have remained similar to those from the LGP (Hinkley and Matsumoto, 2001) or alternatively could have been completely restructured due to the major climate shift. The retreat of the Ross Ice Shelf, 11.5–6 ka, should have had a significant impact upon the dust record, consistent with the dust record at Talos Dome (Delmonte et al., 2010) as hypothetically, storm trajectories and dominant winds would migrate southward to approach TYD from the southeast (Fig. 1).

Sea salt aerosol, is yet another indicator of sea ice and ice shelf extent (Wolff et al., 2003; Lupker et al., 2010); it originates from sea ice covered with brine, frost flowers and bubble bursting over seawater. Here we measure the isotopic and elemental characteristics of the soluble fraction (<0.2 μm) of the TYD ice core for comparison to the insoluble fraction, which is comprised of dust between 0.2 and 30 μm in diameter. Particles larger than 30 μm in diameter were not measured due to the low dust availability and instrumental detection limitations.

This work presents the first detailed Sr and Nd isotopic dataset of coastal Antarctic ice core dust during the last deglaciation. We employ a newly developed mass spectrometry technique utilizing 10^{13} Ohm resistors which can effectively measure variations in Nd isotope composition of extremely small samples to the fourth decimal place (Koornneef et al., 2014). The goals of the study are: (1) to provide the first high-resolution record of dust deposited in East Antarctica during the last deglaciation and into the Holocene, (2) identify and compare the geochemical (radiogenic isotope compositions and rare earth element concentrations) and physical characteristics (dust concentration and particle size) of ice core dust to PSAs from SSA and the Ross Sea sector (e.g. McMurdo Dry Valleys), (3) explore the effects of the retreating Ross Ice Shelf upon regional storm trajectories using the dust record preserved in the TYD ice core, and (4) establish the likely sources of dust to TYD during the LGP and the Holocene.

2. Materials and methods

2.1. Ice core processing

A series of 17 ice core samples from the TYD ice core (M3C1) were selected between 113 and 391 m depth (see Table 1 for depths and ages). The samples measured here encompass a time period of ∼1.1 to ∼31.4 ka before 1950 A.D. Synchronization of the CO_2 concentration record to EPICA Dome C (EDC) and Dronning Maud Land (EDML) ice cores provided chronological refinement of the TYD ice core to approximately 20 ka (Monnin et al., 2004). Recent work has refined the TYD age-scale (Baggenstos, 2015) based on combining the work of Monnin et al. (2004) to 20 ka, and Ahn and Brook (2007) to 60 ka. The updated age scale of Baggenstos (2015) is indistinguishable from the original Brook et al. (2000) age scale for 20–40 ka, the time period encompassing the oldest sample in this study. We use the Monnin et al. (2004) timescale for 1–20 ka and Brook et al. (2000) for 20–60 ka.

Each sample is approximately 660 g and 22 cm long and spans between ∼3 and ∼30 yrs. The ice was cut into 3 longitudinal samples for radiogenic isotope, REE, and dust concentration and size distribution analysis, respectively. The REE and dust concentration and size distribution samples were cut latitudinally into two subsamples (labeled 'a' and 'b', see Tables S1–S4) to obtain a higher temporal resolution. Decontamination and melting occurred in class 10 laminar flow hoods at the University of Michigan. To remove the outer layer and potential contamination each ice sample was scraped using acid-cleaned PFA chisels. The sample was then rinsed using ultra-pure distilled ethanol (Acros Organics) and subsequently rinsed twice with MilliQ water.

2.1.1. REE and dust concentration sample preparation

The traditional "acid leach" REE portion of each sample was triple rinsed with MilliQ water using acid pre-cleaned LDPE calipers and melted in pre-cleaned LDPE Nalgene bottles following procedures established by Boutron et al. (1990). The meltwater was immediately acidified in 1% HNO_3 (ultra-pure) for approximately 1 month prior to analysis. The "full digestion" REE portion consisted of 100 µL taken from each insoluble and soluble sample digested and dissolved in 1 ml of 6M HCl. The samples were subsequently dried down and acidified in 1% v/v HNO_3 for comparison to the traditional "acid leach" REE portion of ice core samples.

The dust concentration and size distribution samples were triple rinsed with MilliQ water using acid pre-cleaned LDPE calipers and stored frozen in triple rinsed PFTE centrifuge tubes until just prior to analysis following the procedures described in Delmonte et al. (2004a).

2.1.2. Radiogenic isotope sample preparation

Ice core sections for radiogenic isotope analysis were buffered to neutral pH during melting with ultra-pure optima grade ammonia (Fischer Scientific) to prevent the dissolution of mineral particles (Aciego et al., 2009). Immediately afterwards, melted samples were filtered through pre-cleaned 0.2 µm and 30 µm filters (particles greater than 30 µm were not measured due to dust availability and analytical limitations). The filtered water (we operatively define as the "soluble fraction" and denote as 'W') was collected in a pre-cleaned Teflon beaker for analysis.

Insoluble fractions (denoted as 'F') were dissolved directly off the 0.2 µm filters using ultra-pure HCl, aqua regia, and HNO_3–HF acid for "total digestion" portions, whereas the soluble fraction was dried under nitrogen flow and infrared radiation before dissolution in ultra-pure 9 M HCl acid for chemistry (Aciego et al., 2009).

Finally, aliquots of both soluble and insoluble fractions (denoted as 'W' and 'F' respectively) were also chemically separated using -ion-exchange columns and Eichrom resins following established procedures of Aciego et al. (2009) and Aarons et al. (2013) for Sr and Nd isotopic analysis. For a full description of sample preparation see Fig. 2.

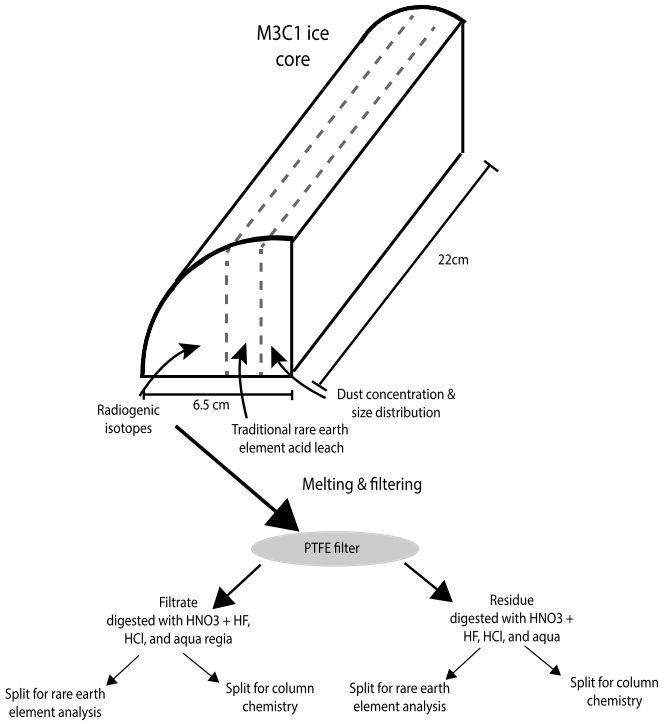

Fig. 2. Schematic of ice core sample preparation for radiogenic isotope and rare earth element analysis of insoluble and soluble portion of TYD ice core. ∗ Insoluble portion of ice core is mineral dust and soluble portion is filtered ice, denoted as 'F' and 'W' respectively.

2.2. PSA sample processing

We use PSA samples from the East Antarctic ice sheet margin for source to sink analyses of TYD ice core dust to PSA dust from the Ross Sea Region. The Ross Sea Region PSAs were selected from the fine fraction of regolith, exposed glacial deposits, and sediments below the surficial deflation eolic pavement (1–3 cm) (Blakowski et al., in press). Approximately 10 mg of each sample were digested in concentrated HF in a Savillex Teflon beaker inside a steel-jacketed Parr acid digestion bomb at 220 °C for 48 h. The insoluble PSA samples were then dried down and immersed in 6M HCl at 180 °C for 12–24 h, dried down, and dissolved in 1 mL of 9M HCl. Sample aliquots of 100 µL were extracted and dried down prior to being re-acidified in 1% HNO_3. The acid leach method for the ice samples is: acidification in 1% HNO_3 (ultra-pure) for approximately 1 month prior to analysis consistent with the methods from Uglietti et al. (2014).

2.3. REE concentration analysis

The REE concentrations of TYD ice were measured using ICP-SFMS (Element 2, Thermo Scientific) coupled with a micro-flow nebulizer and desolvation system (Apex Q) in the clean laboratory at the Byrd Polar and Climate Research Center at The Ohio State University following the procedures in Gabrielli et al. (2006, 2010). REE detection is at the sub-pg g^{-1} levels (Gabrielli et al., 2006), with procedural blanks concentrations 61 and 7.5 times smaller than sample concentrations for the traditional leaching and full acid digestion method respectively (see Table S3).

Table 1
Radiogenic isotope compositions of Taylor Dome ice samples. ε_{Nd} and $^{87}Sr/^{86}Sr$ isotopic compositions of ice core samples measured in this study, top depth and age are noted. Ages are based upon synchronization of CO_2 record in TYD, EDC and EDML ice cores (Monnin et al., 2004). 'F' and 'W' are insoluble and soluble portions.

Sample ID	Top depth (m)	Ice age (ka)	$^{87}Sr/^{86}Sr \pm 2\sigma\ 10^{-6}$	$^{14i}Nd/^{144}Nd \pm 2\sigma\ 10^{-6}$	$\varepsilon_{Nd} \pm 2\sigma\ 10^{-6}$
113F	113.12	1.1	0.712856 (227)	0.512296 (129)	−6.7 (2.5)
113W	113.12	1.1	0.710033 (65)	0.512286 (191)	−6.9 (3.7)
136F	136.12	1.5	0.708418 (540)	–	–
136W	136.12	1.5	0.710078 (86)	0.511948 (126)	−13.5 (2.5)
176F	176.10	2.2	0.708323 (297)	–	–
176W	176.10	2.2	–	0.512297 (130)	−6.7 (2.5)
208F	208.13	3.1	0.714972 (115)	0.512436 (191)	−3.9 (3.7)
208W	208.13	3.1	0.709012 (50)	0.512111 (277)	−10.3 (5.4)
266F	264.80	4.8	0.705428 (33)	0.512446 (163)	−3.8 (3.2)
266W	264.80	4.8	0.705152 (33)	0.512368 (137)	−5.3 (2.7)
281F	279.48	5.3	0.716308 (259)	0.512273 (75)	−7.1 (1.5)
281W	279.48	5.3	0.705353 (21)	0.512360 (84)	−5.4 (1.6)
296F	294.68	6.0	0.706593 (46)	–	–
296W	294.68	6.0	0.710128 (33)	0.512242 (89)	−7.7 (1.7)
299F	297.50	6.1	0.709332 (178)	–	–
299W	297.50	6.1	0.710383 (57)	0.512282 (74)	−6.9 (1.4)
308F	306.50	6.5	0.710751 (244)	0.512594 (170)	−0.9 (3.3)
308W	306.50	6.5	0.707023 (38)	0.512347 (62)	−5.7 (1.2)
323F	321.5	7.3	0.709708 (168)	0.512550 (87)	−1.7 (1.7)
323W	321.5	7.3	0.709522 (75)	0.512333 (93)	−6.0 (1.8)
340F	339.14	9.4	0.713616 (229)	0.512509 (132)	−2.5 (2.6)
340W	339.14	9.4	0.710054 (64)	0.512496 (71)	−2.8 (1.4)
349F	347.6	10.5	–	–	–
349W	347.6	10.5	0.709885 (38)	0.512227 (86)	−8.0 (1.7)
366F	364.60	13.0	0.712416 (98)	0.512398 (194)	−4.7 (3.8)
366W	364.60	13.0	0.709389 (72)	0.512588 (165)	−1.0 (1.4)
376F	374.70	15.5	0.705225 (28)	0.512544 (47)	−1.8 (0.9)
376W	374.70	15.5	0.708497 (74)	0.512595 (54)	−0.8 (1.1)
381F	380.3	19.7	0.710116 (24)	0.512505 (8)	−2.6 (0.15)
381W	380.3	19.7	0.709255 (39)	0.512427 (53)	−4.1 (1.0)
383F	381.5	20.7	0.708974 (9)	0.512459 (62)	−3.5 (1.2)
383W	381.5	20.7	0.710059 (5)	0.512583 (25)	−1.1 (0.5)
392F	391.12	31.4	0.708714 (35)	0.512591 (71)	−0.9 (1.4)
392W	391.12	31.4	0.708950 (77)	0.512605 (47)	−0.6 (0.9)

2.4. Dust concentration and size distribution analysis

Dust concentration and size distribution measurements were conducted by Coulter® Counter at the University of Milan as in Delmonte et al. (2002) and kept frozen until analysis. For each dust concentration and size distribution subsample ~20 ml was available for Coulter® Counter microparticle concentration and size distribution measurements in the range of 1.006–29.83 μm.

2.5. Strontium and neodymium isotope analyses

Chemically separated Sr and Nd were measured using thermal ionization mass spectrometry (TIMS) equipped with 10^{11} Ohm resistors for $^{87}Sr/^{86}Sr$ ratios and 10^{13} Ohm resistors for $^{143}Nd/^{144}Nd$ ratios. Sr isotopic compositions were measured on the University of Michigan Thermo Scientific Triton Plus TIMS and normalized to $^{88}Sr/^{86}Sr = 8.375209$ to account for mass bias. The Sr isotopic standard NBS987 (100 ng) long-term average is $^{87}Sr/^{86}Sr = 0.710245 \pm 17$ (2σ SD, $n = 268$). The USGS reference material BCR-2 (10 ng) measured concurrently with samples averaged 0.705002 ± 37 (2σ SD, $n = 3$), which agrees with published BCR-2 values (0.705013, 0.705000; Aciego et al., 2009 and Jweda et al., 2015 respectively).

The majority of Nd isotopic compositions were measured on a Thermo Scientific Triton *Plus* TIMS using low-noise 10^{13} Ohm resistors at the Vrije Universiteit in Amsterdam and normalized to $^{146}Nd/^{144}Nd = 0.7219$ using the exponential law and mass 147 was monitored to detect any Sm interference (Koornneef et al., 2014). USGS reference material BCR-2 (1 ng) measured concurrently with the samples averaged 0.512634 ± 32 (2σ SD, $n = 2$), in agreement with measured values in Jweda et al. (2015) of $^{143}Nd/^{144}Nd = 0.512637$. The $^{143}Nd/^{144}Nd$ ratio of isotopic standard CIGO (100 pg) was measured simultaneously at $^{143}Nd/^{144}Nd = 0.511344 \pm 49$ (2σ SD, $n = 5$), close to the long-term average value of $^{143}Nd/^{144}Nd = 0.511334 \pm 10$ (2σ SD, $n = 28$) (Koornneef et al., 2014), demonstrating that 10^{13} Ohm resistors can effectively measure variations in $^{143}Nd/^{144}Nd$ to the fourth decimal place for samples as small as 100 pg. Two LGP samples (381 and 383) were measured on a Thermo Scientific Triton *Plus* TIMS using standard 10^{11} Ohm resistors at the University of Michigan and normalized to $^{146}Nd/^{144}Nd = 0.7219$ using the exponential law and mass 149 was monitored to detect any Sm interference. BCR-2 (10 ng) measured concurrently with the samples averaged 0.512642 ± 42 (2σ SD, $n = 4$), similar to measured values (Jweda et al., 2015). The long-term average for JNdi-1 is 0.512101 ± 12 (2σ SD, $n = 110$).

3. Results

The dust concentration and size distribution, REE, Na and Sr concentrations of the fifteen ice core sections are summarized in Tables S1, S3, and S4 respectively. The dust flux calculations and the sample information for Ross Sea Region PSAs are presented in Tables S2 and S5 respectively. Sr and Nd isotopic composition of the TYD dust and ice samples are summarized in Table 1.

3.1. Dust concentration and size distribution

Dust concentrations are >500 and <15 ppb during glacial and interglacial periods respectively (Fig. S1), which is similar to dust concentrations observed in interior Antarctic ice cores (e.g. Delmonte et al., 2002, 2004a, 2007, 2008). In the 1–5 μm, 1–10 μm,

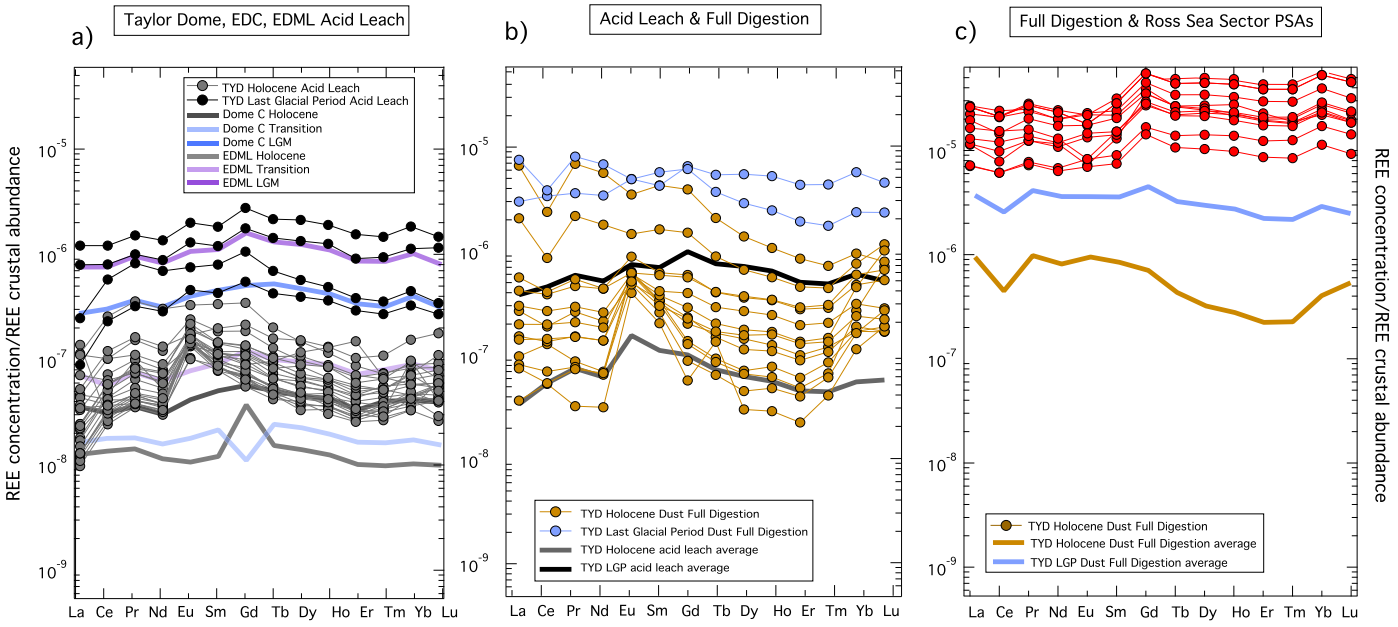

Fig. 3. Rare earth element concentrations of TYD dust in ice. a) Normalized REE concentrations with respect to the mean crustal abundance (Wedepohl, 1995) in the 13 LGP and Holocene acid leached TYD ice samples with REE normalized concentrations of ice from EDC, and EDML also separated by time periods (Gabrielli et al., 2010; Wegner et al., 2012). b) Comparison of average acid leached and fully digested TYD ice. c) Comparison of average fully digested TYD ice to Ross Sea sector potential source area dust (Blakowski et al., in press).

and 1–20 μm dust diameter size range, the dust concentrations range from ~9–537 ppb, 14–541 ppb, and 14–544 ppb respectively.

The mean mass TYD dust particle diameter calculated using volume distribution increases with decreasing depositional age (Table S1). Our measured mean mass TYD Holocene dust particle diameter (~3 μm) is larger than the glacial dust particle diameter (~1.8 μm). The two oldest glacial samples, from ~31.4–15.5 ka are lognormally distributed with a modal value of ~2 μm, consistent with the long-range transported dust observed in the Talos Dome ice core (Delmonte et al., 2010; Albani et al., 2012). To explore the difference in grain size distributions further, we use the proportion of fine particles (fine particle percentage, or FPP) and coarse particles (coarse particle percentage, or CPP) with respect to the total mass as defined in Delmonte et al. (2004b). Samples from the Holocene (~1.1–10.5 ka) on average have a high CPP greater than 2 μm (~85%) than older samples (~13–31.4 ka) with a CPP of ~69% (Table S1).

Larger dust particle diameters observed during the Holocene is also observed at Talos Dome, a coastal ice core in East Antarctica (Albani et al., 2012) and the West Antarctic Ice Sheet (WAIS) Divide deep ice core (Koffman et al., 2014a). The dust input at TYD, Talos Dome and WAIS Divide during the Holocene is dominated by larger dust particles whereas the dust concentration during the LGP is attributed to finer dusts.

The dust flux rates at TYD are determined using the variable water equivalent accumulation rates (calculated from ice equivalent) for each time period (Morse et al., 1998) and dust concentration (this study) (see Table S2, Fig. 4). On average, the flux of dust particles between 1–20 μm during the LGP was ~3.9 $mg\,m^{-2}\,yr^{-1}$ compared to ~2.3 $mg\,m^{-2}\,yr^{-1}$ during the Holocene. The average flux of dust particles between 1–5 μm and 1–10 μm was ~3.6 and ~3.7 $mg\,m^{-2}\,yr^{-1}$ during the LGP and decreased to ~1.1 and ~1.5 $mg\,m^{-2}\,yr^{-1}$ during the Holocene (Table S2). The dust flux record of fine particles (1–5 μm) at TYD follows a similar pattern observed at EDC, however the change in TYD dust flux across the termination of the LGP is smaller (Fig. 4). The flux of larger dust particles (up to 20 μm) is significantly higher during the Holocene compared to the LGP (Fig. 4). The difference in dust flux between the TYD and EDC ice cores is substantial, however the overall trend is similar (Fig. 4). The dust flux in the most recent portion of the TYD record is comparable to WAIS Divide ice core (Koffman et al., 2014a), however comparison to older sections is not yet available. When compared to the Talos Dome record (Albani et al., 2012), the dust flux is slightly higher in the TYD record during the Holocene, but the difference in dust flux from the two ice cores between the LGP and Holocene is distinctive, most notably in the coarse dust particle portion.

3.2. Rare Earth Element concentrations

3.2.1. REE concentrations of TYD insoluble fraction

REEs serve as a valuable tool for characterizing mineral dust in Antarctic ice, and we differentiate between light REEs (LREEs: La, Ce, Pr, Nd), medium REEs (MREEs: Sm, Eu, Gd, Tb, Dy, Ho), and heavy REEs (HREEs: Er, Tm, Yb, Lu). The REE concentrations of the TYD ice were normalized to the mean upper continental crustal abundance of each element (Wedepohl, 1995) (Fig. 3). Comparable shapes of REE patterns could indicate uniform dust sources (or uniform mixing of sources); whereas departures from a constant pattern could indicate a change in dust source(s). The REE concentrations of the TYD samples follow the dust concentrations for glacial/interglacial REE concentrations in other Antarctic ice cores (Gabrielli et al., 2010; Wegner et al., 2012). Higher input of continental dust during glacial periods results in higher REE concentrations observed in glacial samples compared to interglacial samples. All of the samples from the Holocene display a unique positive Eu anomaly (Fig. 5b), which is not found in Holocene samples in ice cores from the interior East Antarctic ice sheet (Gabrielli et al., 2010; Wegner et al., 2012).

3.2.2. REE concentrations of TYD soluble fraction

The REE concentrations of the full-digestion soluble and insoluble fractions follow similar but not identical patterns (Fig. S4). REE concentrations of the LGP ice samples are higher than the majority of the Holocene samples and have a unique positive Eu anomaly. Another sample (1.1 ka, sample 113) has a pronounced enrichment in Pr not observed in any other soluble samples (Fig. 6). We would

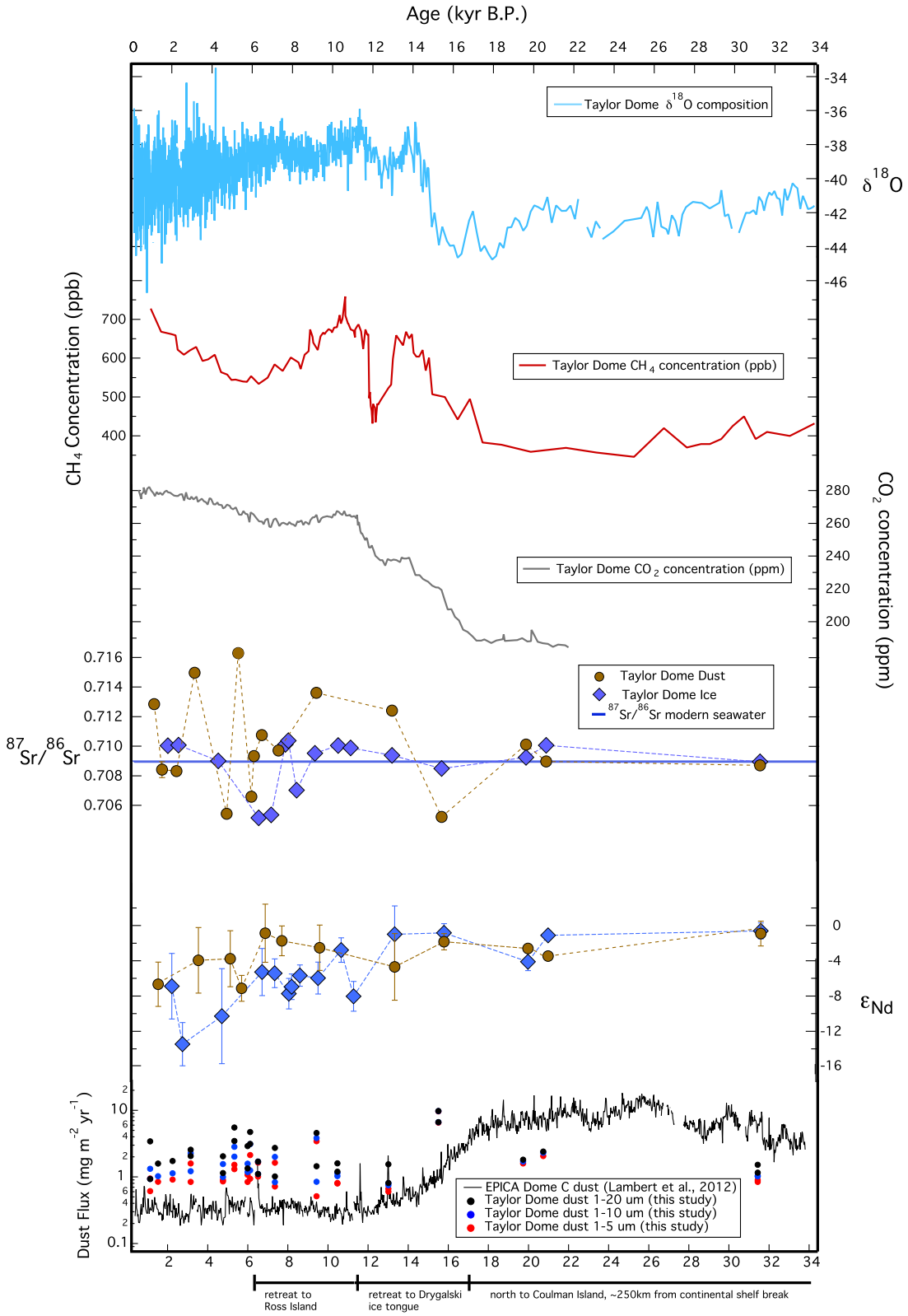

Fig. 4. Thirty-two-thousand-year climate history of the Ross Sector of East Antarctica. TYD ice core $\delta^{18}O$ isotope profile (blue line; Steig et al., 2000), CH_4 concentration (red line; Brook et al., 2000), CO_2 concentration (grey line; Monnin et al., 2004), Sr and Nd isotopic compositions (brown circles = dust fraction, blue diamonds = ice fraction) and the Sr isotopic composition of modern seawater (solid blue line) (Hodell et al., 1990). TYD dust flux record for three different size fractions (red circles = 1–5 μm, blue circles = 1–10 μm, and black circles = 1–20 μm, this work) with EDC dust flux (black line; Lambert et al., 2012). (For interpretation of the references to color in this figure legend, the reader is referred to the web version of this article.)

expect the REE composition of the soluble fraction of TYD ice to be similar to seawater, however only Antarctic Bottom water REE data exists in current literature (Kawabe et al., 1998). The REE composition of the soluble fraction of TYD ice and Antarctic Bottom water do not match (Fig. 6).

3.2.3. REE concentrations of potential source area dust

We include 76 PSA dust samples from the Ross Sea Sector (Baroni et al., 2008; Delmonte et al., 2010) from 17 locations along the north-central Transantarctic Mountains, the ice-free valleys and nunataks of Victoria Land and nearby McMurdo Sound sector for source-to-sink comparison. The bedrock ranges from late Proterozoic to early Paleozoic granites and gneisses, Devonian to Triassic Beacon Supergroup sedimentary rocks and the sills of the Jurassic Ferrar dolerite (Blakowski et al., in press; Stump and Fitzgerald, 1992). The sampled material ranges from regolith, glacial dunes, lacustrine sand, and volcanic material. See Supplementary Table S5 for more detailed information on the sample geologic history, geographic surroundings, climate and collection. The REE concentrations of the PSA dust from the Ross Sea Sector display a uniform crustal pattern (Fig. 3c), with a slight enrichment of heavy REE with respect to light REE.

3.3. Sr and Nd isotopic compositions

We use the radiogenic isotopic composition of dust entrained in TYD ice to discern the shifts in provenance during the time period studied. The isotope variability in the glacial samples is large: $^{87}Sr/^{86}Sr$ = 0.7052–0.7101 and ε_{Nd} = −3.5 to −0.9, whereas Holocene dust displays an even broader range: $^{87}Sr/^{86}Sr$ = 0.7054–0.7163 and ε_{Nd} = −7.1 to −0.9. We observe significant variations in the ε_{Nd} compositions of the Holocene soluble fraction; the insoluble and soluble fractions from a single sample are not coupled and suggest that the variable soluble ε_{Nd} compositions are not a result of leaching from the insoluble fraction (Fig. 4). The majority of soluble samples measure close to the established $^{87}Sr/^{86}Sr$ seawater composition of 0.70917 (Hodell et al., 1990) with the exception of samples from ~4.7, 5.3, and 6.5 ka (0.705152, 0.705353, and 0.707023 respectively). Most of the insoluble samples possess a higher Sr radiogenic isotope composition than the water-soluble fraction (Fig. 4).

The TYD insoluble portion spans a broad range of Sr and Nd isotopic compositions (Fig. 5). The majority of the Holocene samples are more radiogenic with respect to Sr (average Holocene = 0.710573 versus average LGP = 0.708257), and plot closer to the regional Ross Sea Region patterns (colored areas, Fig. 5). However, at least 3 of the Holocene samples plot within the SSA source area. The glacial samples plot further away from the Ross Sea Region source area pattern (with the exception of a sample from ~13 ka, which may be a result of the deglacial transition), also observed in dust from a previously measured East Antarctic ice core (Delmonte et al., 2004a, 2008).

4. Discussion

4.1. Dust concentration, flux and size distribution: evidence of a changing regional climate

Long-term variations in dust concentration and flux have been noted in records from the EDC ice core from interior East Antarctica (Lambert et al., 2008). The EDC ice core records a drastic drop (an order of magnitude) in dust flux (Fig. 4) and dust concentration (Fig. S2) following the termination of the LGP (Delmonte et al., 2004a). Similarly, the flux, concentration and size distribution of TYD ice core dust changes dramatically from the LGP to the Holocene, with larger dust particles more prevalent during the

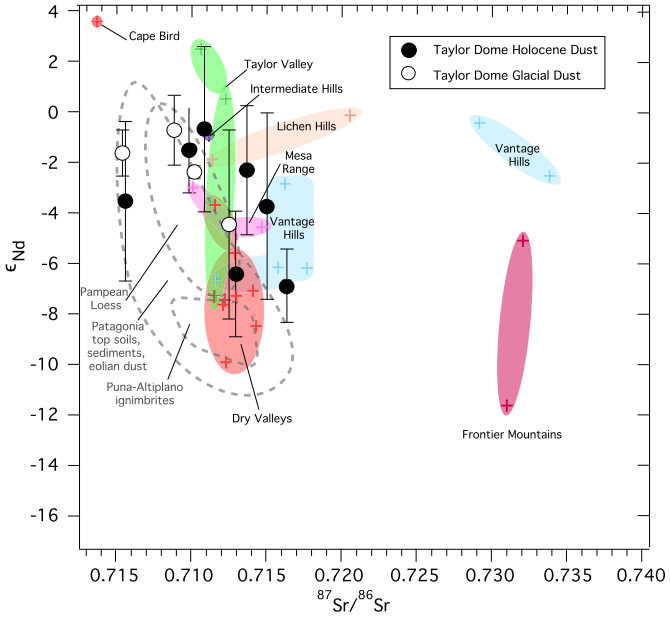

Fig. 5. Radiogenic isotopic compositions of Taylor Dome ice core dust and regional Potential Source Areas. Sr and Nd isotopic compositions of Taylor Dome ice core Holocene (black circles) and Glacial dust (white circles) with regional Potential Source Areas plotted in various colors (colored crosses are individual data points) (Delmonte et al., 2010, 2013; Blakowski et al., in press) and long range Potential Source Area of Southern South America plotted within dashed gray line (Delmonte et al., 2004a; Gaiero, 2007).

Holocene. The higher total Holocene dust flux was also observed in the Talos Dome ice core (Albani et al., 2012). This higher input of large dust particles suggests more local input of dust, which can be attributed to an alteration in storm trajectories and dominant weather pathways (Morse et al., 1998). The ice-free terrains of Victorialand and the nearby Transantarctic Mountains during the last glacial period rule out the possibility of increased large dust particle concentration due to a reduction of land ice cover and resulting exposure of local dust sources (Delmonte et al., 2010).

The difference in dust flux between the TYD and EDC ice cores is significant (Fig. 4). The overall trends of dust flux in both ice cores are similar: higher (lower) proportion of fine particle flux during LGP (Holocene), though the magnitude of difference is less in the TYD core most likely due to the proximity to unglaciated terrains. However, due to the discontinuous record of the TYD core, it is difficult to speculate as to the underlying causes of the dust flux differences between the TYD and EDC ice cores.

The measurement of size variations of dust particles entrained in ice cores has proven useful for inferring changes in dust transport pathways and atmospheric circulation (Delmonte et al., 2004b). The modal diameter in the TYD glacial samples is ~2 μm, consistent with previous results obtained from another coastal East Antarctic ice core (Talos Dome) (Albani et al., 2012), as well as interior East Antarctic ice cores (Vostok, EDC) (Petit et al., 1999; Delmonte et al., 2004a). The small dust diameters observed in ice cores across East Antarctica during the LGP are indicative of long-range sourced dust that was most likely deposited congruently throughout East Antarctica (Petit et al., 1999; Delmonte et al., 2004a; Albani et al., 2012).

The modal diameter of Holocene dust in the TYD ice core is larger at ~3 μm, and the samples are not log-normally distributed—most likely due to poor size-sorting during transport and deposition. In contrast, ice cores from interior East Antarctica (Dome B, Komsomolskaia, EDC) during the time period of 12 ka have smaller average dust particle diameters ranging from 1.8, 1.9, and 2.2 μm respectively (Delmonte et al., 2004b). Talos Dome, a

coastal ice core, is characterized by poor size sorting during the Holocene and the presence of dust particles in the size range of 5–10 μm is strong evidence of local input (Albani et al., 2012). Analysis of the TYD dust size distribution in three size fractions (1–5, 1–10, and 1–20 μm respectively) highlights the shift in average dust particle diameter between the LGP and the Holocene (Fig. S2).

4.2. Rare Earth Element signatures of Taylor Dome ice

The REE patterns normalized to upper continental crustal abundance are consistent with input of dust from continental sources (Fig. 5a). The normalization is applied to the samples and results in a characteristic REE profile with a clear positive Eu anomaly for Holocene samples (Fig. 3). Any deviations from this pattern would be indicative of a change in source area, which is best determined by comparing these results to the REE profiles of soil and rock from hypothesized source areas (see Fig. 3c).

The REE patterns (both the acid leached and fully digested samples) for the TYD ice core display a similar, temporally unchanging profile throughout the LGP. There is a distinct change (positive Eu anomaly) for samples younger than ~15.5 ka (sample 376), although a Holocene sample (~6.1 ka, sample 299) displays a pattern similar to LGP samples (Fig. 3). The positive Eu anomaly observed in the TYD Holocene samples (Fig. 3a, b) is also observed in young volcanic PSA dust from Patagonia (Gaiero, 2004), however it is unlikely that the TYD Holocene dust is originating from Patagonia as the isotopic compositions are not in agreement (Fig. S7). The comparison of the results of the two REE methods is described below.

4.2.1. Comparison of traditional acid leaching to full acid digestion

The results of different sample methodology for REE and trace element analysis is an important topic still under consideration (Rhodes et al., 2011; Koffman et al., 2014b). Previous work highlighted the importance of sample methodology upon the measured trace element and REE concentrations; different laboratories may use varying methods for sample preparation and subsequent analysis which may result in incorrect or misleading measured concentrations due to incongruent elemental dissolution of trace and REEs (Rhodes et al., 2011; Koffman et al., 2014b; Uglietti et al., 2014). Previous work using three separate preparations (acid leached, pre-filtered then acid leached, and full digestion) of Antarctic ice-core samples to determine REE concentrations demonstrated that glacial–interglacial variations of the REE patterns emerge and are significant if the method adopted is consistently used for all the samples analyzed (Gabrielli et al., 2010). In our study, the REE patterns of the acid leached and fully digested TYD samples vary from one another: the LREE patterns in the higher concentrated samples (LGP) are distinctively different, whereas the lower concentrated samples (Holocene) all display the positive Eu anomaly (Fig. 3b).

When using the trace element concentrations to discern changes in atmospheric trace elements due to anthropogenic pollution and/or land use changes, the sample preparation method becomes more important for comparing ice core records (Koffman et al., 2014b; Uglietti et al., 2014). The results of these studies emphasize the importance of allowing melted acidified ice core samples to sit for at least one month prior to analysis, and that incomplete dissolution of minerals and/or incongruent leaching is an issue that can be resolved by full acid digestion using HF. To discern the effects of acid leaching versus full acid digestions on our TYD ice core samples we used both techniques (Fig. 3b). Our results demonstrate that full acid digestion results in higher REE concentrations than the acid leaching method by nearly one order of magnitude (as described above in methods), and comparison of both techniques yielded varying REE concentration patterns (Fig. 3), which also occurred in earlier work measuring trace element concentration (Koffman et al., 2014b). The full digestion Holocene TYD samples all display a unique Eu enrichment anomaly, with the exception of the sample from the time period of ~6.1 ka (sample 299). The fully digested LGP TYD samples do not have this positive Eu anomaly, supporting the hypothesis that dust deposited on TYD during the dust origin during the LGP is different than during the Holocene. Prior work comparing the acid leaching method to the full acid digestion method determined that the traditional acid leaching method overestimates the LREE concentrations with respect to the MREE and HREE concentrations (Gabrielli et al., 2010). In contrast, the leached TYD samples possess lower normalized La concentrations compared to the fully digested samples (Fig. 3b). The results presented here demonstrate that the sample methodology of traditional acid leaching versus full acid digestion produces distinctly different REE concentrations.

4.2.2. REE comparison of Taylor Dome dust to PSAs

Reconstruction of dust sources and pathways through time is possible through the comparison of REE patterns in ice cores to those measured in PSAs (Wegner et al., 2012). We compare the fully digested acid leach data of TYD dust to Ross Sea sector PSA dust samples as both sets of data were processed the same. The REE concentrations of TYD LGP samples are distinctly different from the REE patterns of the Ross Sea sector PSA samples (Fig. 3c). The Holocene TYD ice has a significant positive Eu anomaly not observed in the Ross Sea sector PSA samples; however, both sets of samples have a similar HREE pattern with the exception of the sample from ~6.1 ka (sample 299) (Fig. 3c). Based on the REE pattern during the Holocene, we hypothesize that the source of dust to TYD during this time period is a consistent mix of dust from PSAs in the Ross Sea Sector and a small but constant input of long-range transported dust. The REE pattern of dust deposited in Antarctic ice throughout the last deglaciation suggests an input of a mixed long-range transported dust or input from a baseline source such as SSA (Gabrielli et al., 2010; Wegner et al., 2012). The Holocene REE patterns of EDC and EDML ice differs significantly (high enrichment in Gd) from those of the Ross Sea sector PSAs and the Holocene TYD samples, implying that the source of dust to East Antarctica during the Holocene changes based upon the proximity to the coast (Delmonte et al., 2013; Bertler et al., 2005) (Fig. 3c). The Holocene TYD REE pattern remains relatively uniform and constant, and may be a reflection of dust input from a local unrecognized (unmeasured) source. The current Holocene storm trajectory approaching TYD from the southeast crosses the Royal Society Range, which has not been sampled for chemical characterization of the PSA and therefore cannot be ruled out as a potential contributor of dust to TYD (Fig. 1).

We evaluate the possibility of dust contribution from both the Ross Sea sector and SSA PSAs with a simple two-component mixing model of REE concentrations in increments of 10% (i.e. 90% SSA dust input and 10% Ross Sea sector dust input) (Fig. S5). The HREE enrichment of Ross Sea sector and SSA PSAs is not observed in the average measured Holocene REE concentrations or the modeled mixtures of SSA and Ross Sea sector REE concentrations (Fig. S5). The discrepancy between the observed average TYD Holocene REE concentrations and the PSAs from the Ross Sea sector and SSA may be attributed to dust input from an uncharacterized source or fractionation of REEs during long-range transport. Changes in the mineral composition may occur during eolian transport due to gravitational sorting: heavy minerals settle out of the atmosphere closer to the source, leaving behind suspended particles depleted in HREE, Zr and Hf (Gaiero, 2007; Aarons et al., 2013).

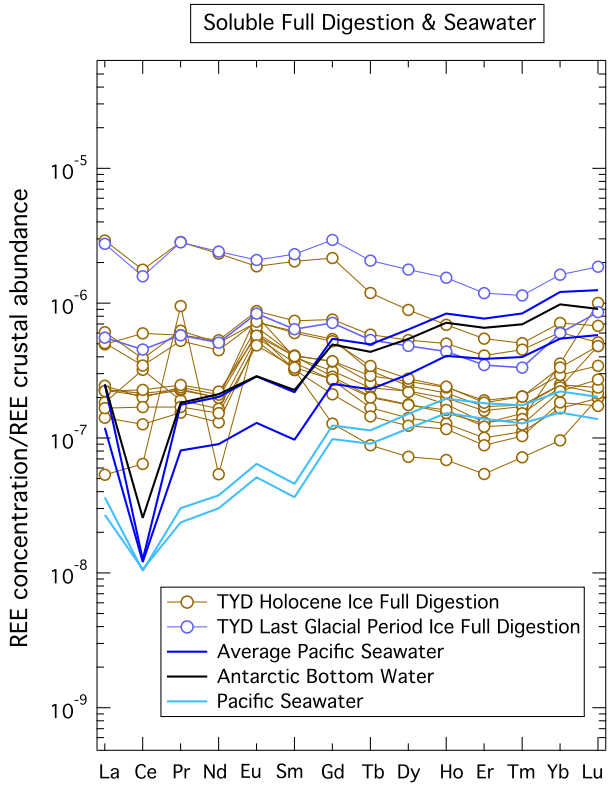

Fig. 6. Rare earth element concentrations of Taylor Dome ice soluble portion (full digestion) in comparison to REE concentrations in seawater (Kawabe et al., 1998). Hollow brown and blue circles are Holocene and Last Glacial Period fully digested samples. Solid dark blue, black and light blue lines are average Pacific seawater, Antarctic bottom water, and unique Pacific seawater samples respectively (Kawabe et al., 1998). (For interpretation of the references to color in this figure legend, the reader is referred to the web version of this article.)

4.2.3. REE concentration of TYD soluble portion

As a first hypothesis, the higher REE concentrations observed during the LGP compared to the Holocene may be attributed to the increased formation, transport and deposition of sea-salt aerosol originating from sea ice, as is the case for other Antarctic ice core records (Petit et al., 1999; Wolff et al., 2006). We would expect the REE pattern of the soluble LGP samples to most closely resemble the REE pattern of Antarctic seawater, represented by a solid black line in Fig. 6. This is not the case. So it is possible that aerosol mineral dust and unbufferable minerals smaller than 0.2 μm may be present in the soluble portion of the TYD ice core (as the melted ice core was filtered to a size of 0.2 μm) along with oceanic derived aerosols (dissolved sea salt), and leached elements from the dust fraction during transport and ice core sample processing (Lupker et al., 2010). To explore the relative contribution of sea salt versus mineral dust to the soluble REE patterns observed in the TYD ice core record, a two-component mixing model in increments of 10% (i.e. 90% mineral dust and 10% sea salt contribution), is utilized (Fig. S6). This two-component model does not produce the measured REE concentration pattern, which suggests that other processes are occurring during either transport or ice formation that may fractionate REE patterns. Further, this modeling confirms that leaching from mineral dust is unlikely after deposition.

4.3. Isotopic signature of Taylor Dome and East Antarctic dust

Previous work utilizing Sr isotopes as a tracer of aerosol mineral dust highlighted the importance of separating soluble and insoluble portions of samples to accurately interpret dust provenance (Aarons et al., 2013). The measured trace element (TE) concentrations of TYD ice are another indicator of changes in sea salt contribution and we use the Na/Sr ratio to serve as a proxy (Table S4). The average insoluble and soluble TYD Na/Sr ratios are 191 and 1034 respectively (Fig. S3). The average upper continental crust and seawater Na/Sr ratio is 81 (Wedepohl, 1995) and 1358 (Riley and Tongudai, 1967) respectively, which supports the conclusion that the higher soluble Na/Sr ratio in the TYD samples is attributable to sea salt acting as the primary constituent (Fig. S3). It is likely that sea salt originating from nearby seasonal sea ice in the Ross Sea is a large contributor to the soluble Sr in the TYD ice, and we therefore interpret our radiogenic isotope data separately as the soluble and insoluble portions.

4.3.1. Radiogenic isotopic composition of soluble portion

The water-soluble portions of the TYD ice core plot close to the modern $^{87}Sr/^{86}Sr$ composition of seawater, and the highest variability occurs between ~8–4 ka (Fig. 4). It is unclear why three water-soluble samples are not in agreement with the established $^{87}Sr/^{86}Sr$ composition of seawater (0.70917, Hodell et al., 1990). However, the variable ε_{Nd} compositions of Holocene soluble samples could be attributed to oceanic processes, the Southern Ocean ε_{Nd} composition close to the Ross Sea ranges from −11.3 to −8.4 (Albarède et al., 1997). Aerosols originating from seasonal sea ice with frost flowers during warmer, interglacial conditions may cause the transition from uniform to variable ε_{Nd} values (Fig. 4).

4.3.2. Radiogenic isotopic composition of insoluble portion

The Sr and Nd isotopic compositions of TYD dust indicate a shift provenance from a relatively constant long-range input to a more variable proximal source following the deglaciation, as the Holocene isotopic compositions trend more towards the PSAs from the Ross Sea sector. In general, the Holocene samples span a larger range of $^{87}Sr/^{86}Sr$ and ε_{Nd} isotope values, and appear to be comprised of a combination of Ross Sea sector PSAs. The hypothesized Holocene storm trajectory crosses the Royal Society Range (Fig. 1), and it has not been sampled or analyzed for $^{87}Sr/^{86}Sr$ and ε_{Nd} isotopic compositions. The unsampled and unmeasured Royal Society Range along with additional unidentified proximal sources cannot be ruled out as the predominant source of Holocene dust. The dust from the LGP however, appears to be less radiogenic with respect to Nd, and lies closer to the SSA source area (Basile et al., 1997) as concluded by previous studies (Delmonte et al., 2004a, 2010).

4.3.3. Synthesis of physical and chemical characteristics of mineral dust

The dust size distribution in TYD ice transitions from fine to coarse during the last deglaciation, signifying a transition from distal to local dust sources. The REE concentrations clearly distinguish different dust sources during the LGP and Holocene, and the presence of a distinct positive Eu anomaly in almost all of the Holocene samples suggest that the interglacial samples are originating from a similar source area with congruent bedrock geology. Finally, the radiogenic isotope measurements also imply that the dust sources to TYD during the Holocene are similar to local sources (Fig. 5), and are most likely a combination between isotopically characterized and uncharacterized areas in the Ross Sea Sector. During the LGP we observe isotopic compositions similar to dust from SSA, which supports a shift from long-range transported dust to a local source. The change in dust sources may be attributed to a change of dominant storm trajectories, and is consistent with the hypothesis that the moisture-bearing storms approaching TYD have shifted from the north to the southeast following the last deglaciation.

4.3.4. Retreat of Ross ice shelf reflected in dust record

Glaciological studies (Morse et al., 1998; Hinkley and Matsumoto, 2001) suggest that the Ross Ice Shelf retreat discernable in paleo-records caused a shift in the local storm trajectories and

the composition of aerosols delivered to the region. Geochemical records of spelothems in northern Europe provide evidence for movement in predominant storm trajectories as a result of shifting Late-Pleistocene Northern Hemisphere ice shelf extents (Luetscher et al., 2015), thereby confirming that geochemical evaluation of paleoclimate proxies may reveal small-scale shifts in climate (e.g. storm tracks). Major and rare earth element concentrations of TYD ice indicate that total impurities were at their highest and dust deposition was greater than sea salt during the LGP (Hinkley and Matsumoto, 2001), perhaps a result of increased dust availability in South America (Basile et al., 1997; Delmonte et al., 2004a, 2010; Gabrielli et al., 2010; Wegner et al., 2012). The sea salt concentration increased in the dust–salt mixture at the termination of the LGP (Hinkley and Matsumoto, 2001), suggesting an increase in new sea ice (covered in brine and frost flowers) extent but unchanged wind strength and patterns as the dust composition remained uniform. A reversal in the dust–sea salt concentrations indicates that the sea ice extent briefly returned to LGP conditions between 10–11 ka, before a final retreat and subsequent change to sea-salt dominance of aerosol composition. Synthesizing the work of Morse et al. (1998) and Hinkley and Matsumoto (2001) confirms that the Ross Ice Shelf retreat had a profound impact on the local climate – changing both storm trajectories and the composition of aerosols deposited on the local surroundings, which is supported by the data presented here.

The broad range of radiogenic isotopic compositions of dust from Holocene ice demonstrates the variable sources of dust to TYD during this time period. It is possible that the sources of dust to TYD during the LGP originated from more than one distal source, however it appears that during the Holocene the dust provenance and dust transport pathways are more variable.

5. Conclusions

We present geochemical and physical measurements of dust in the TYD ice core record spanning the LGP, the deglaciation and the Holocene. In addition to providing the first high time resolution radiogenic isotope compositions of dust in an East Antarctic ice core, we also utilize and compare two methods of REE sample processing (acid leach and full digest). The results presented here demonstrate that the two sample methodologies produce distinctly different REE concentrations, which has implications for studies comparing and contrasting REE concentrations in ice core records. The geographic location of TYD relative to the Ross Ice Shelf provides an ideal study site to explore local shifts in storm trajectories related to the rapid retreat of the Ross Ice Shelf during the last deglaciation. Our data supports an alteration in local circulation following the termination of the LGP and the subsequent transition into the Holocene as evidenced by the shifts in dust particle diameters, REE concentrations, and radiogenic isotope compositions. The systematic shift in radiogenic isotope composition combined with an increase in dust particle diameter during the Holocene suggests that the dust transported to Taylor Dome is originating from a local source. These observations are consistent with previous studies of a coastal East Antarctic ice core (Delmonte et al., 2010; Albani et al., 2012). We attribute this modification in dominant weather pathways to the retreat of the Ross Ice Shelf, as first proposed by Morse et al. (1998).

Acknowledgements

This work was funded by grants from the Rackham Graduate School and the Turner Award from the Department of Earth and Environmental Sciences at the University of Michigan to S.M. Aarons and from NSF OPP Antarctic Glaciology Award 1246702 to S.M. Aciego and P. Gabrielli. We thank C. Bouman for assistance in the development of 10^{-13} Ohm resistors for small samples. This research is the Byrd Polar and Climate Research center publication 1544. We thank the logistics and drilling team at Taylor Dome, C. Uglietti for laboratory assistance, and two anonymous reviewers for their helpful comments.

Appendix A. Supplementary material

Supplementary material related to this article can be found online at http://dx.doi.org/10.1016/j.epsl.2016.03.035.

References

Aarons, S.M., Aciego, S.M., Gleason, J.D., 2013. Variable Hf–Sr–Nd radiogenic isotopic compositions in a Saharan dust storm over the Atlantic: implications for dust flux to oceans, ice sheets and the terrestrial biosphere. Chem. Geol. 349–350, 18–26.

Aciego, S.M., Bourdon, B., Lupker, M., Rickli, J., 2009. A new procedure for separating and measuring radiogenic isotopes (U, Th, Pa, Ra, Sr, Nd and Hf) in ice cores. Chem. Geol. 266.

Ahn, J., Brook, E.J., 2007. Atmospheric CO_2 and climate from 65 to 30 ka B.P. Geophys. Res. Lett. 34 (L10), 703. http://dx.doi.org/10.1029/2007GL029551.

Albani, S., Delmonte, B., Maggi, V., Baroni, C., Petit, J.R., Stenni, B., Mazzola, C., Frezzotti, M., 2012. Interpreting last glacial to Holocene dust changes at Talos Dome (East Antarctica): implications for atmospheric variations from regional to hemispheric scales. Clim. Past 8, 741–750.

Albarède, F., Goldstein, S.L., Dautel, D., 1997. The neodymium isotopic composition of manganese nodules from the Southern and Indian oceans, the global oceanic neodymium budget, and their bearing on deep ocean circulation. Geochim. Cosmochim. Acta 61 (6), 1277–1291.

Anderson, J.B., Shipp, S.S., Bartek, L.R., Reid, D.E., 1992. Evidence for a grounded ice sheet on the Ross Sea continental shelf during the late Pleistocene and preliminary paleodrainage reconstruction. In: Elliot, D. (Ed.), Contributions to Antarctic Research III. In: Antarctic Research Series, vol. 57. American Geophysical Union, Washington, D.C.

Baggenstos, D., 2015. Taylor Glacier as an archive of ancient ice for large-volume samples: chronology, gases, dust, and climate. Ph.D. thesis. University of California, San Diego.

Baroni, C., Fasano, F., Giorgetti, G., Salvatore, M.C., Ribecai, C., 2008. The Ricker Hills Tillite provides evidence of oligocene warm-based glaciation in Victoria Land, Antarctica. Glob. Planet. Change 60, 457–470.

Basile, I., Grousset, F.E., Revel, M., Petit, J.R., Biscaye, P.E., Barkov, N.I., 1997. Patagonian origin of glacial dust deposited in East Antarctica (Vostok and Dome C) during glacial stages 2, 4 and 6. Earth Planet. Sci. Lett. 146, 573–589.

Beghin, P., Charbit, S., Dumas, C., Kageyama, M., Roche, D.M., Ritz, C., 2014. Interdependence of the growth of the Northern Hemisphere ice sheets during the last glaciation: the role of atmospheric circulation. Clim. Past 10, 345–358.

Bertler, N., et al., 2005. Snow chemistry across Antarctica. Ann. Glaciol. 41 (1), 167–179.

Blakowski, M.A., Aciego, S.M., Delmonte, B., Baroni, C., Salvatore, M.C., Sims, K.W.W., in press. Sr–Nd–Hf isotope characterization of dust source areas in Victoria Land and the McMurdo Sound sector of Antarctica. Quat. Sci. Rev. http://dx.doi.org/10.1016/j.quascirev.2016.03.023.

Boutron, C.F., Patterson, C.C., Barkov, N.I., 1990. The occurrence of zinc in Antarctic ancient ice and recent snow. Earth Planet. Sci. Lett. 101, 248–259.

Brook, E.J., Harder, S., Severinghaus, J., Steig, E.J., Sucher, C.M., 2000. On the origin and timing of rapid changed in atmospheric methane during the last glacial period. Glob. Biogeochem. Cycles 14, 559–572.

Cook, K.H., Held, I.M., 1988. Stationary waves of the ice age climate. J. Climate 1, 807–819.

Delmonte, B., Andersson, P.S., Hansson, M., Schoberg, H., Petit, J.R., Basile-Doelsch, I., Maggi, V., 2008. Aeolian dust in East Antarctica (EPICA-Dome C and Vostok): provenance during glacial ages over the last 800 kyr. Geophys. Res. Lett. 35, L07703. http://dx.doi.org/10.1029/2008GL033382.

Delmonte, B., Baroni, C., Andersson, P.S., Narcisi, B., Salvatore, M.C., Petit, J.R., Scarchilli, C., Frezzotti, M., Albani, S., Maggi, V., 2013. Modern and Holocene aeolian dust variability from Talos Dome (Northern Victoria Land) to the interior of the Antarctic ice sheet. Quat. Sci. Rev. 64, 76–89.

Delmonte, B., Baroni, C., Andersson, P.S., Schoberg, H., Hansson, M., Aciego, S., Petit, J.R., Albani, S., Mazzola, C., Maggi, V., Frezzotti, M., 2010. Aeolian dust in the Talos Dome ice core (East Antarctica, Pacific/Ross Sea sector): Victoria Land versus remote sources over the last two climate cycles. J. Quat. Sci. 25, 1327–1337.

Delmonte, B., Basile-Doelsch, I., Petit, J.R., Maggi, V., Revel-Rolland, M., Michard, A., Jagoutz, E., Grousset, F., 2004a. Comparing the Epica and Vostok dust records during the last 220,000 years: stratigraphical correlation and provenance in glacial periods. Earth-Sci. Rev. 66, 63–87.

Delmonte, B., Petit, J.R., Andersen, K.K., Basile-Doelsch, I., Maggi, V., Lipenkov, V.Ya., 2004b. Dust size evidence for opposite regional atmospheric circulation changes over east Antarctica during the last climatic transition. Clim. Dyn. 23, 427–438.

Delmonte, B., Petit, J.R., Basile-Doelsch, I., Jagoutz, E., Maggi, V., 2007. Late quaternary interglacials in East Antarctica from ice-core dust records. In: Clim. Past. Interglacials, vol. 7, pp. 53–73.

Delmonte, B., Petit, J.R., Maggi, V., 2002. LGM-Holocene changes and Holocene millennial-scale oscillations of dust particles in the EPICA Dome C ice core, East Antarctica. Ann. Glaciol. 35, 306–312.

Francis, J.A., Chan, W., Leathers, D.J., Miller, J.R., Veron, D.E., 2009. Winter northern hemisphere weather patterns remember summer Arctic sea-ice extent. Geophys. Res. Lett. 36. http://dx.doi.org/10.1029/2009GL037274.

Gabrielli, P., Barbante, C., Turetta, C., Marteel, A., Boutron, C., Cozzi, G., Cairns, W., Ferrari, C., Cescon, P., 2006. Direct determination of rare earth elements at the subpicogram per gram level in antarctic ice by ICP-SFMS using a desolvation system. Anal. Chem. 78, 1883–1889.

Gabrielli, P., Wegner, A., Petit, J.R., Delmonte, B., De Deckker, P., Gaspari, V., Fischer, H., Ruth, U., Kriews, M., Boutron, C., Cescon, P., Barbante, C., 2010. A major glacial interglacial change in aeolian dust composition as inferred from rare earth elements in Antarctic ice. Quat. Sci. Rev. 29, 265–273.

Gaiero, D.M., 2004. The signature of river-and wind-borne materials exported from Patagonia to the southern latitudes: a view from REEs and implications for paleoclimatic interpretations. Earth Planet. Sci. Lett. 219, 357–376.

Gaiero, D.M., 2007. Dust provenance in Antarctic ice during glacial periods: from where in southern South America? Geophys. Res. Lett. 34, L17707.

Grootes, P.M., Steig, E.J., Stuiver, M., Waddington, E.D., Morse, D.L., 1994. A new ice core record from Taylor Dome, Antarctica. Eos Trans. AGU 75, 225.

Grousset, F.E., Biscaye, P.E., 2005. Tracing dust sources and transport patterns using Sr, Nd and Pb isotopes. Chem. Geol. 222, 147–167.

Hall, B.L., Denton, G.H., Heath, S.L., Jackson, M.S., Koffman, T.N.B., 2015. Accumulation and marine forcing of ice dynamics in the western Ross Sea during the last deglaciation. Nat. Geosci. 8, 625–628.

Hall, N.M.J., Valdes, P.J., Dong, B., 1996. The Maintenance of the Last Great Ice Sheets: a UGAMP GCM Study. J. Climate 9, 1004–1019.

Hammer, C., Clausen, H., Dansgaard, W., Neftel, A., Kristinsdottir, P., Johnson, E., 1985. Continuous impurity analysis along the Dye-3 deep core. In: Geophys. Monog. Series, vol. 33, pp. 90–94.

Harris, J.M., 1992. An analysis of 5 day midtropospheric flow patterns for the South Pole. Tellus B 20, 115–120.

Hinkley, T.K., Matsumoto, A., 2001. Atmospheric regime of dust and salt through 75,000 years of Taylor Dome ice core: refinement by measurement of major, minor, and trace metal suites. J. Geophys. Res. 106, 18,487–18,493.

Hodell, D.A., Mead, G.A., Mueller, P.A., 1990. Variation in the strontium isotopic composition of seawater (8 Ma to present): implications for chemical weathering rates and dissolved fluxes to the oceans. Chem. Geol. 80, 291–307.

Jouzel, J., Vaikmae, R., Petit, J.R., Martin, M., Duclos, Y., Stievenard, M., Lorius, C., Toots, M., Melieres, M.A., Burckle, L.H., Barkov, N.I., Kotlyakov, V.M., 1995. The two-step shape and timing of the last deglaciation in Antarctica. Clim. Dyn. 11, 151–161.

Jweda, J., Bolge, L., Class, C., Goldstein, S.L., 2015. High Precision Sr–Nd–Hf–Pb Isotopic Compositions of USGS Reference Material BCR-2. Geostand. Geoanal. Res. http://dx.doi.org/10.1111/j.1751-908X.2015.00342.x.

Kageyama, M., Valdes, P.J., 2000. Impact of the North American ice-sheet orography on the Last Glacial Maximum eddies and snowfall. Geophys. Res. Lett. 27, 1515.

Kawabe, I., Toriumi, T., Ohta, A., Miura, N., 1998. Monoisotopic REE abundances in seawater and the origin of seawater tetrad effect. Geochem. J. 32, 213–229.

Koffman, B.G., Handley, M.J., Osterberg, E.C., Wells, M.L., Kreutz, K.J., 2014b. Dependence of ice-core relative trace-element concentration on acidification. J. Glaciol. 60 (219), 103–112.

Koffman, B.G., Kreutz, K.J., Breton, D.J., Kane, E.J., Winski, D.A., Birkel, S.D., Kurbatov, A.V., Handley, M.J., 2014a. Centennial-scale variability of the Southern Hemisphere westerly wind belt in the eastern Pacific over the past two millennia. Clim. Past 10, 1125–1144.

Koornneef, J.M., Bouman, C., Schwieters, J.B., Davies, G.R., 2014. Measurement of small ion beams by thermal ionisation mass spectrometry using new 10^{13} Ohm resistors. Anal. Chim. Acta 819, 49–55.

Laîné, A., Kageyama, M., Salas-Mélia, D., Voldoire, A., Rivière, G., Ramstein, G., Planton, S., Tyteca, S., Peterschmitt, J.Y., 2008. Northern hemisphere storm tracks during the last glacial maximum in the PMIP2 ocean-atmosphere coupled models: energetic study, seasonal cycle, precipitation. Clim. Dyn. 32, 593–614.

Lambert, F., Bigler, M., Steffensen, J.P., Hutterli, M., Fischer, H., 2012. Centennial mineral dust variability in high-resolution ice core data from Dome C, Antarctica. Clim. Past 8, 609–623.

Lambert, F., Delmonte, B., Petit, J.R., Bigler, M., Kaufmann, P.R., Hutterli, M.A., Stocker, T.F., Ruth, U., Steffensen, J.P., Maggi, V., 2008. Dust-climate couplings over the past 800,000 years from the EPICA Dome C ice core. Nature 452, 616–619.

Liakka, J., Nilsson, J., 2010. The impact of topographically forced stationary waves on local ice-sheet climate. J. Glaciol. 56 (197), 534–544.

Licht, K.J., Jennings, A.E., Andrews, J.T., Williams, K.M., 1996. Chronology of late Wisconsin ice retreat from the western Ross Sea, Antarctica. Geology 24 (3), 223–226.

Luetscher, M., Boch, R., Sodemann, H., Spotl, C., Cheng, H., Edwards, R.L., Frisia, S., Hof, F., Muller, W., 2015. North Atlantic storm track changes during the Last Glacial Maximum recorded by Alpine spelothems. Nat. Commun. 6. http://dx.doi.org/10.1038/ncomms7344.

Lupker, M., Aciego, S.M., Bourdon, B., Schwander, J., Stocker, T.F., 2010. Isotopic tracing (Sr, Nd, U and Hf) of continental and marine aerosols in an 18th century section of the Dye-3 ice core (Greenland). Earth Planet. Sci. Lett. 295, 277–286.

McGee, D., Broecker, W.S., Winckler, G., 2010. Gustiness: the driver of glacial dustiness? Quat. Sci. Rev. 29, 2340–2350.

Monnin, E., Steig, E.J., Siegenthaler, U., Kawamura, K., Schwander, J., Stauffer, B., Stocker, T.F., Morse, D.L., Barnola, J.-M., Bellier, B., Raynaud, D., Fischer, H., 2004. Evidence for substantial accumulation rate variability in Antarctica during the Holocene, through synchronization of CO_2 in the Taylor Dome, Dome C and DML ice cores. Earth Planet. Sci. Lett. 224, 45–54. http://dx.doi.org/10.1016/j.epsl.2004.05.007.

Morse, D.L., 1997. Glacier geophysics at Taylor Dome, Antarctica. Ph.D. thesis. University of Washington.

Morse, D.L., Waddington, E.D., Steig, E.J., 1998. Ice age storm trajectories inferred from radar stratigraphy at Taylor Dome, Antarctica. Geophys. Res. Lett. 25, 3383–3386.

Petit, J.R., Jouzel, J., Raynaud, D., Barkov, N.I., Barnola, J.M., Basile, I., Bender, M., Chappellaz, J., Davis, M., Delaygue, G., Delmotte, M., Kotlyakov, V.M., Legrand, M., Lipenkov, V.Y., Lorius, C., Pepin, L., Ritz, C., Saltzman, E., Stievenard, M., 1999. Climate and atmospheric history of the past 420,000 years from the Vostok ice core, Antarctica. Nature 399, 429–436.

Rhodes, R.H., Baker, J.A., Millet, M.-A., Bertler, N.A.N., 2011. Experimental investigation of the effects of mineral dust on the reproducibility and accuracy of ice core trace element analyses. Chem. Geol. 286, 207–221.

Riley, J.P., Tongudai, M., 1967. The major cation/chlorinity ratios in sea water. Chem. Geol. 2, 263–269.

Rivière, G., Laîné, A., Lapeyre, G., Salas-Mélia, D., Kageyama, M., 2010. Links between Rossby wave breaking and the North Atlantic Oscillation–Arctic Oscillation in present-day and Last Glacial Maximum climate simulations. J. Climate 23, 2987–3008.

Steig, E.J., Morse, D.L., Waddington, E.L., Stuiver, M., Grootes, P.M., Mayewski, P.A., Twickler, M.S., Whitlow, S.I., 2000. Wisconsinan and Holocene climate history from an ice core at Taylor Dome, western Ross Embayment, Antarctica. Geogr. Ann., Ser. A 82A (2–3), 213–235.

Stump, E., Fitzgerald, P.G., 1992. Episodic uplift of the Transantarctic Mountains. Geology 20 (2), 161–164.

Uglietti, C., Gabrielli, P., Lutton, A., Olesik, J., Thompson, L., 2014. Large variability of trace element mass fractions determined by ICP-SFMS in ice core samples from worldwide high altitude glaciers. Appl. Geochem. 47, 109–121.

Vihma, T., 2014. Effects of Arctic Sea ice decline on weather and climate: a review. Surv. Geophys. 35 (5), 1175–1214.

Wedepohl, K.H., 1995. The composition of the continental crust. Geochim. Cosmochim. Acta 59, 1217–1232.

Wegner, A., Gabrielli, P., Wilhelms-Dick, D., Ruth, U., Kriews, M., De Deckker, P., Barbante, C., Cozzi, G., Delmonte, B., Fischer, H., 2012. Change in dust variability in the Atlantic sector of Antarctica at the end of the last deglaciation. Clim. Past 8 (1), 135–147.

Wolff, E.W., Fischer, H., Fundel, F., Ruth, U., Twarloh, B., Littot, G.C., Mulvaney, R., Rothlisberger, R., de Angelis, M., Boutron, C.F., Hansson, M., Jonsell, U., Hutterli, M.A., Lambert, F., Kaufmann, P., Stauffer, B., Stocker, T.F., Steffensen, J.P., Bigler, M., Siggaard-Andersen, M.L., Udisti, R., Becagli, S., Castellano, E., Severi, M., Wagenbach, D., Barbante, C., Gabrielli, P., Gaspari, V., 2006. Southern Ocean sea-ice extent, productivity and iron flux over the past eight glacial cycles. Nature 440, 491–496.

Wolff, E.W., Rankin, A.M., Röthlisberger, R., 2003. An ice core indicator of Antarctic sea ice production? Geophys. Res. Lett. 30. http://dx.doi.org/10.1029/2003gl018454.